Spectroscopic properties of photorefractive $BaTiO_3$ double doped with cerium and rhodium

Robert N. Schwartz and Barry A. Wechsler*
HRL Laboratories, LLC, 3011 Malibu Canyon Road, Malibu, California 90265
(Received 13 July 1999)

We have grown and characterized crystals of $BaTiO_3$ double doped with Ce and Rh. This material has defect charge states that can easily be manipulated by illumination with different wavelengths of light and may have potential for nonvolatile holographic storage using a two-step, sensitized recording scheme. Electron paramagnetic resonance (EPR), photo-EPR, optical absorption, and light-induced optical-absorption measurements were used to identify the charge states, probe the electronic structure, and locate the ionization levels associated with the Ce and Rh centers relative to the band edges of the $BaTiO_3$ host. In addition, the effects of illumination at various wavelengths on the defect states were used to develop a qualitative sensitization model.

I. INTRODUCTION

The use of photorefractive crystals, including $BaTiO_3$, $LiNbO_3$, and $(Sr,Ba)Nb_2O_6$, for holographic data storage has been known for more than 30 years.[1] In this application, data are stored in the form of refractive index gratings recorded with laser beams capable of producing photoionization in the material. The transport, via drift and diffusion, and subsequent trapping of photocarriers produces a charge density distribution that mimics the intensity of the incident interference pattern. The modulation of the internal electric space-charge field is subject to erasure both by dark conduction and by light-induced charge redistribution. The latter effect is particularly troublesome for data storage applications because the readout of stored data produces at least partial erasure.

A number of approaches have been studied to improve the storage properties of such materials.[2] In particular, methods to make the photorefractive gratings nonvolatile, i.e., insensitive to erasure during readout and during storage in the dark, have been developed. Among these techniques are thermal fixing, electrical fixing, and two-photon or sensitized recording. Recently, both thermal fixing[3–5] and electrical fixing[6,7] have been demonstrated in nominally undoped $BaTiO_3$ crystals. The only report of sensitized recording in $BaTiO_3$ was that by Buse, Holtmann, and Krätzig[8] who demonstrated short-lived sensitization involving two defect species in a nominally undoped sample. However, the identities of the centers involved were not known, and no attempt was made to optimize the recording process through doping or post-growth annealing.

In sensitized recording,[9] beams at two different wavelengths are required to write a grating. The first beam is a gating (or sensitizing) beam that raises carriers into an excited or metastable state and thus creates absorption at a second wavelength. The write beams at the second wavelength have sufficient photon energy to produce free carriers. Grating formation proceeds through the usual transport mechanisms. Readout is performed at the write wavelength and, with the sensitizing beam absent, the grating is stable against erasure. It should be noted that in order to be useful for long-term storage, the dark conductivity of such crystals must be very low, otherwise the grating storage time will be limited by dark decay. The role of dopants or impurities in controlling the dark conductivity has previously been demonstrated.[10]

Rare-earth elements have been considered the most likely candidates for such two-step recording processes because they may display relatively long-lived excited states which makes it possible to photoionize the species by illumination with a second light beam. Wechsler *et al.*[11] have described an alternate route to nonvolatile storage using double-doped $BaTiO_3$. The two dopants introduce defect levels in the band gap that allow gated photoionization of carriers from levels sensitive to near-IR light and storage of the gratings in a level that is insensitive to infrared radiation. At the same time, the crystal also displays very long dark storage time.

In order to make these materials useful for practical application as storage media, further understanding of the effects of doping and processing upon the optical and electrical properties is needed. Specifically, the ability to control the generation and migration of charge both under illumination and in the dark is required. In this paper we report on the optical, electronic, and photophysical properties of single crystal $BaTiO_3$:Ce,Rh; a ferroelectric oxide material that has unique and favorable properties for holographic storage. We demonstrate the introduction of photochromic behavior in $BaTiO_3$ through double doping and show how this may be used to allow nonvolatile storage of refractive index gratings. Our results are similar to those recently reported by Buse Adibi, and Psaltis,[12] who extended earlier work[13] on $LiNbO_3$:Fe,Mn and used essentially the same sensitized recording method as we discuss here.

This paper is organized as follows: In Sec. II we describe our experimental procedures. The electron paramagnetic resonance (EPR) and optical-absorption measurements and their analysis are presented in Sec. III. A description of sensitized recording in $BaTiO_3$ is presented in Sec. IV. In Sec. V we discuss the implications of our results toward obtaining material optimized for the sensitized recording method of holographic fixing in $BaTiO_3$.

II. EXPERIMENTAL PROCEDURES

$BaTiO_3$ single crystals were grown by the top-seeded solution growth method.[14,15] Dopants were added to the melt in

the form of CeO_2 and RhO_2. Although several crystals with various dopant concentrations were grown, most measurements reported here were obtained on samples of a crystal in which the dopant concentrations were 15 ppm for Ce and 1600 ppm for Rh (expressed as the atomic ratio of Ce/Ba and Rh/Ba in the melt). Individual samples were cut and polished, electrically poled, and then repolished to produce samples for holographic and other studies (with the exception of samples studied by electron paramagnetic resonance, see below, which were not poled and were only polished on one face). Poling was carried out by raising the sample temperature above T_c (132 °C) and then cooling through the phase transition with an electric field of ~1 kV/cm applied along one of the cubic [001] directions.

Most measurements were carried out on ''as-grown'' samples, but in some cases small samples were subjected to post-growth annealing treatments in reducing atmospheres. For these experiments, the crystals were heated at 700 °C in a horizontal tube furnace with a flowing atmosphere of CO and CO_2. The gas mixture was adjusted to provide controlled oxygen partial pressures between approximately 10^{-6} and 10^{-21} bar at the annealing temperature. Following the annealing, the clamshell-type furnace was opened to provide relatively rapid cooling, while the gas mixture continued to flow through the closed furnace tube.

Secondary-ion mass spectrometry (SIMS) analyses were carried out on several samples in order to determine the concentrations of Ce and Rh in the grown crystals. From the SIMS data, we found the distribution coefficient for Ce (i.e., concentration in the crystal/concentration in the melt) to be on the order of 0.05–0.1. In the case of Rh, the distribution coefficient was found to be in the range of 0.0001–0.001.

EPR spectra were recorded at *X* band with a Varian E-109 homodyne spectrometer equipped with a Hewlett-Packard 5342A automatic microwave frequency counter and a proton magnetic resonance gaussmeter for accurately measuring the spectrometer frequency and magnetic field, respectively. For variable temperature measurements between 4.2 K and room temperature, an Oxford Instruments Limited ESR-9 continuous-flow helium cryostat system was used. Single $BaTiO_3$:Ce,Rh crystals with dimensions $1.5\times1.5\times5$ mm^3 were directly illuminated in the microwave cavity by means of an optical fiber. The optical fiber was threaded through the sample holder (2-mm-i.d quartz tube) and positioned so that the cleaved end of the fiber was located approximately 1–2 mm from the polished end-face of the crystal. The incident radiation was provided by either a Schwartz Electro-Optics Ti:sapphire laser or a Coherent Model 590 dye laser pumped by a Coherent Innova 400 Ar^+-ion laser operating at 488/515 nm (multiline mode). The $BaTiO_3$:Ce,Rh crystals retained high optical quality and were intact and crack free even after numerous cooling and warming cycles over the temperature range ~5 to 300 K.

Optical transmission measurements were made at room temperature on a Perkin-Elmer Lambda 9 spectrophotometer. The absorption spectra were obtained from the transmission data and corrected for the Fresnel losses using the index of refraction data reported by Wemple, DiDomenico, and Camlibel.[16]

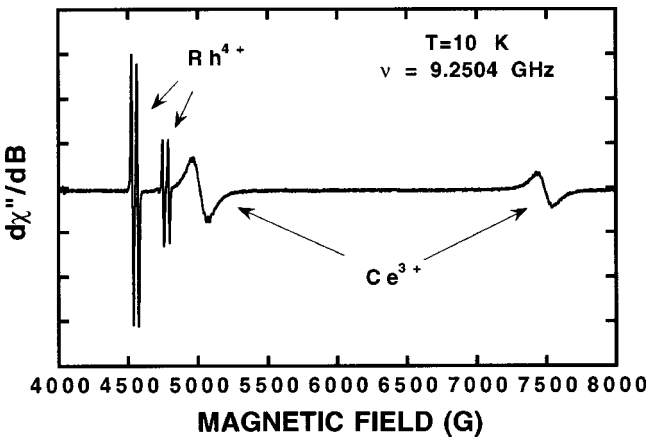

FIG. 1. EPR spectrum of as-grown $BaTiO_3$:Ce,Rh with $\mathbf{B}\|[111]$ direction. Instrumental parameters are as follows: microwave power, ~ 1 mW; modulation amplitude, 2 G.

III. RESULTS

A. EPR

In order to determine the charge states of the dopants EPR measurements were made on as-grown and reduced $BaTiO_3$:Ce,Rh crystals cut from the same boule. Figure 1 shows an EPR spectrum of an as-grown crystal recorded at 10 K with the external magnetic field **B** parallel to the [111] direction. Clearly displayed are two sets of spectral features; one assigned to Rh^{4+} and the other to Ce^{3+}. For the present we will only focus our attention on the Ce^{3+} spectrum, since that assigned to Rh^{4+} has been previously reported in the literature,[17,18] whereas the EPR of Ce^{3+} in $BaTiO_3$ has not, to our knowledge, been reported.

Shown in Fig. 2 is the angular dependence of the magnetic-field resonances $\{B_{\rm res}(\varphi)$; φ is the angle from the [001] direction, solid circles$\}$ assigned to Ce^{3+} ($4f^1$, $^2F_{5/2}$ ground state, $S=\frac{1}{2}$) for variation of the applied magnetic field **B** in the $(\bar{1}10)$ plane. The observed pattern is consistent with trigonal [111] symmetry, which is expected for $BaTiO_3$ at low temperatures, and is discussed in more detail below. It

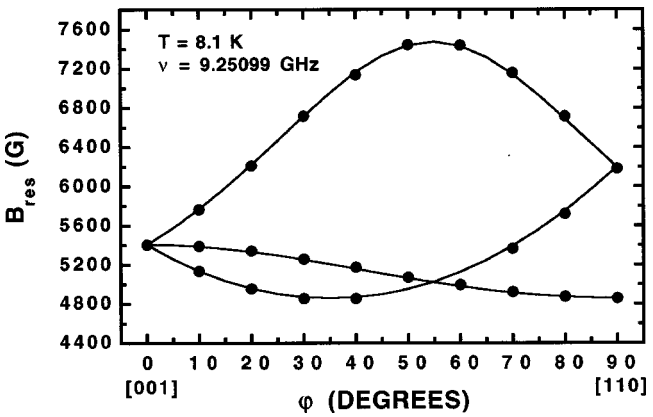

FIG. 2. Angular variation of the EPR resonance transitions of Ce^{3+} in $BaTiO_3$:Ce,Rh for **B** in the $(\bar{1}10)$ plane. The solid circles represent the experimental data; the solid lines are the theoretical curves computed using the measured principal values $|g_\|| = 0.8842$ and $|g_\perp| = 1.3604$.

should be pointed out that this angular variation is similar to that reported for Nd^{3+} in this host.[19]

For Ce^{3+} located at a site with C_{3v} symmetry, the ground state $^2F_{5/2}$ ($J=\frac{5}{2}$) splits into three Kramers's doublets. The spin Hamiltonian in Cartesian form for a system with effective electron spin $S=\frac{1}{2}$ is given by

$$H=\beta[g_{\parallel}S_zB_z+g_{\perp}(S_xB_x+S_yB_y)]. \quad (1)$$

Here β is the Bohr magneton, $g_{\parallel}$ and $g_{\perp}$ are the principal elements of the g matrix, and the S_i's and B_i's are the components of the spin angular momentum operator **S** and the applied magnetic field **B**, respectively, in the coordinate system $i=x,y,z$ for which the g matrix is diagonal.[20] Diagonalization of the above axial symmetric spin Hamiltonian yields an expression for the resonance condition:

$$B_{\rm res}(\vartheta)=[h\nu/g(\vartheta)\beta], \quad (2)$$

where

$$g(\vartheta)=[g_{\parallel}^2\cos^2\vartheta+g_{\perp}^2\sin^2\vartheta]^{1/2}. \quad (3)$$

Here ϑ is the angle between the applied magnetic field **B** and the trigonal axis, i.e., the [111] direction.

There are four [111] directions in the rhombohedral phase of $BaTiO_3$ (psuedocubic; $\alpha=89°51'$).[21] However, when the magnetic field is applied in the $(\bar{1}10)$ plane (or any of the equivalent planes {110}) two of the sites in the $(\bar{1}10)$ plane have axes that are at $+54°44'$ and $-54°44'$ $[\pm\cos^{-1}(1/\sqrt{3})]$ with respect to the [001] direction. These two sites are magnetically inequivalent and give rise to two resonances. The remaining two not lying in the $(\bar{1}10)$ plane are equivalent for all orientations of **B** in the $(\bar{1}10)$ plane and give rise to a single resonance. Thus a maximum of three resonances is seen for arbitrary orientations of the magnetic field in the $(\bar{1}10)$ plane. It should also be noted that when **B** lies along the [001] direction all sites are equivalent and only a single resonance is observed.

The angles for **B**, when confined to the $(\bar{1}10)$ plane, relative to each of the four [111] directions are

$$\vartheta_1=\varphi+\cos^{-1}(1/\sqrt{3}),$$

$$\vartheta_2=\varphi-\cos^{-1}(1/\sqrt{3}), \quad (4)$$

$$\vartheta_3=\vartheta_4=\cos^{-1}(\cos\varphi/\sqrt{3}),$$

where φ is the angle between the applied magnetic field **B** and the [001] direction. Using these expressions for ϑ_i in Eq. (2) and (3), one obtains from a fit to the experimental data $|g_{\parallel}|=0.8842$ and $|g_{\perp}|=1.3604$; the solid curves shown in Fig. 2 represent the computed fit based on these g factors. The magnitudes of these g factors relative to those reported for Ce^{3+} in other hosts, as well as the site location in the $BaTiO_3$ host, is discussed below in Sec. V.

B. Optical absorption

Optical-absorption spectra of as-grown Rh-doped, Ce-doped, and Ce, Rh-doped $BaTiO_3$ crystals are compared in Fig. 3. In the case of the Rh-doped crystal a prominent absorption occurs at ~640 nm (~1.9 eV). The optical and/or

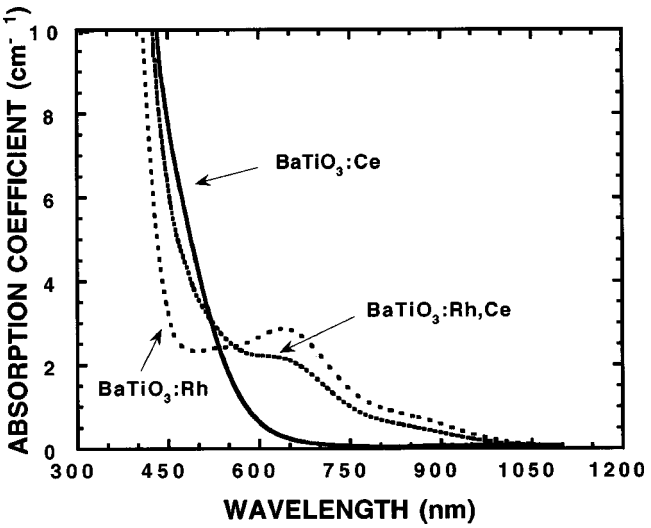

FIG. 3. Optical-absorption spectra of three doped $BaTiO_3$ crystals recorded at room temperature. The light was polarized parallel to the **c** axis. The double-doped sample was exposed to room lights for an indeterminate time before the spectrum was taken.

electronic properties of $BaTiO_3$:Rh have been discussed in the recent literature[18,22,23] and here we will only summarize the pertinent results.

Rhodium, a $4d$ transition metal, may exist in several charge states ($4d^{n+}$) and spin configurations in $BaTiO_3$. Since the $4d$ electrons are less tightly bound than $3d$ electrons, the strong-crystal field[24] approximation is applicable for interpreting the optical spectra of Rh ions. $Rh^{3+}(4d^6)$ is the most stable charge state and hence, the most extensively studied. Its ground state in perfect O_h symmetry (neglecting spin-orbit coupling) is $^1A_{1g}\{(t_{2g})^6\}$, with singlet excited states $^1T_{1g}\{(t_{2g})^5(e_g)\}$ and $^1T_{2g}\{(t_{2g})^5(e_g)\}$.[25,26] For these states the spins are all paired; therefore, diamagnetic behavior is expected. Rh^{2+} and Rh^{4+} have been less extensively studied. Both have paramagnetic ground states and both have been observed by EPR spectroscopy.[27,28] In the strong-crystal-field approximation[24] the ground state of $Rh^{2+}(4d^7)$ is $^2E_g\{(t_{2g})^6(e_g)\}$,[27,29] and for $Rh^{4+}(4d^5)$ the ground state is $^2T_{2g}\{(t_{2g})^5\}$.[27] Recently $Rh^{5+}(4d^4)$ has been identified in $BaTiO_3$:Rh by Kröse *et al.*[22,23] In O_h symmetry the ground state, again in the strong-crystal-field approximation, is $^3T_{1g}\{(t_{2g})^4\}$. Even though the Rh^{5+} ion is an $S=1$ spin system, it appears to be EPR-silent over the range of temperatures investigated.[22,23] It is well known that for $(4d^n)$ ions, the spin-orbit coupling $\zeta(\vec{l}\cdot\vec{S})$ is of the same order of magnitude as the crystal-field splitting.[24] This favors strong coupling of the spin system to the lattice, and thus leads to extremely short electron spin-lattice relaxation times, which in turn, manifests in the broadening of the resonance signal beyond direction.

Since internal transitions, i.e., $d\rightarrow d^*$, are in general weak because they are Lapporte forbidden,[24] the strong optical-absorption peaking at ~1.9 eV in as-grown $BaTiO_3$:Rh is assigned as a charge-transfer transition. This absorption involves the promotion of an electron from the oxygen $2p$ orbitals which make up the valence-band edge, to levels in the band gap associated with the Rh^{4+} ion. Alternatively, this

transition may be viewed as the photoionization of holes to the valence band according to the reaction

$$Rh^{4+} + \hbar\omega \rightarrow Rh^{3+} + h^{+}_{VB}. \quad (5)$$

It has also been established that the Rh^{5+} ion in $BaTiO_3$:Rh has an optical-absorption band centered at ~775 nm (~1.6 eV).[22,23] This absorption is likewise assigned as a charge-transfer transition, which can be described by the equation

$$Rh^{5+} + \hbar\omega \rightarrow Rh^{4+} + h^{+}_{VB}. \quad (6)$$

Ce^{3+} ($4f^1$) has a simple energy-level structure; it consists of only two multiplets, with ground-state assignment $^2F_{5/2}$ and the excited state $^2F_{7/2}$. Since the $4f$ electrons are highly shielded by the outer $5s$ and $5p$ shells of electrons, the optically active $4f$ electrons are not strongly affected by neighboring ligands. Thus in most hosts the separation between these two multiplets is ~2200 cm^{-1} (~0.27 eV) and therefore optical absorption occurs in the infrared. Ce^{3+} has, however, a strong broad UV absorption peaking at ~28 000 cm^{-1} (~3.5 eV). These transitions fall into two categories:[30,31] (i) $4f \rightarrow 5d$ transitions and (ii) charge transfer, which involves the promotion of an electron from, for example in $BaTiO_3$, the oxygen $2p$ orbitals (valence-band edge) to the partly filled $4f$ orbitals of the Ce^{3+}. As indicated above these bands can be quite broad, especially if $5d$ orbitals are involved, since they are strongly coupled to the ligand environment.

C. Light-modified optical absorption

The optical-absorption spectra of several $BaTiO_3$:Ce,Rh crystals were measured after dark relaxation and during or following illumination with an optical source external to the optical spectrophotometer. Since these samples were highly light sensitive, both in intensity and wavelength, the illuminating radiation is referred to below as the *sensitizing radiation* and the modified optical absorption of the sample following or during illumination as the *sensitized state*. In addition, photo-EPR measurements were made on selected samples.

The optical-absorption spectrum of a sample before and after exposure to white light from a microscope illuminator is shown in Fig. 4. Prior to illumination, the absorption spectrum is similar to that of $BaTiO_3$:Ce (see Fig. 3). In the sensitized state the crystal shows the absorption feature near 640 nm that is characteristic of Rh^{4+}. Note the extended absorption in the infrared. Above ~900 nm the absorption is almost exclusively due to the sensitization of the crystal. We have found that sensitizing of the crystal with laser light or focused light is not necessary; ordinary room lighting sensitizes the crystal, though more slowly. A heat lamp is effective in quickly returning the crystal to its desensitized (dark) state. Light-induced absorption changes are illustrated in Fig. 5, where the change in absorption at 1.01 μm is shown during and after illumination with a 488/515 nm Ar^+-ion laser. Exposure to blue-green light produces a strong increase in the absorption of the 1.01-μm probe beam; this absorption is quickly ''bleached'' when the blue-green beam is turned off. Note that in the absence of the 1.01-μm probe beam, the absorption change induced by the blue-green illumination has a lifetime of more than 10 h.

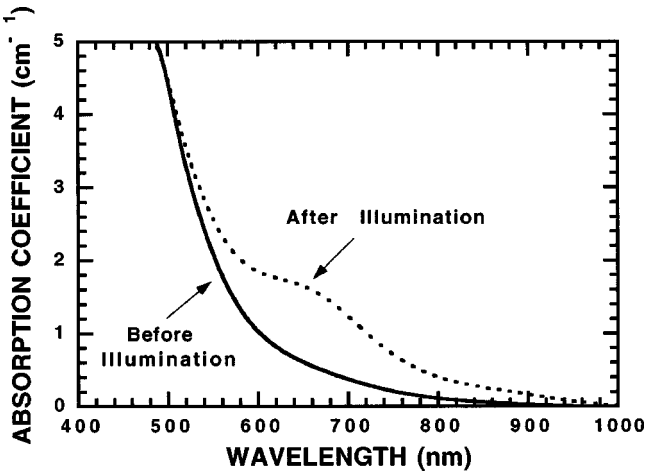

FIG. 4. Optical-absorption spectra recorded at room temperature of $BaTiO_3$:Ce,Rh before and after illumination with a microscope illuminator. The light was polarized parallel to the **c** axis.-

IV. SENSITIZED GRATING FORMATION

A. Ionization levels

Optical and EPR spectroscopic data provide detailed information concerning the location of the ionization levels of deep impurities relative to the band edges of the host. Recent work by Wechsler *et al.*[18] and Kröse *et al.*[22,23] locate the ionization levels associated with the various Rh^{n+} charge states as illustrated in Fig. 6. In the case of Ce^{n+}, the dark-decay measurements of Bacher *et al.*[10] locate a Ce-related ionization level nearly midgap in $BaTiO_3$ (see Fig. 6).

B. Sensitization model

The main features of this energy level scheme have been described by Wechsler *et al.*[11] and are mentioned here to aid

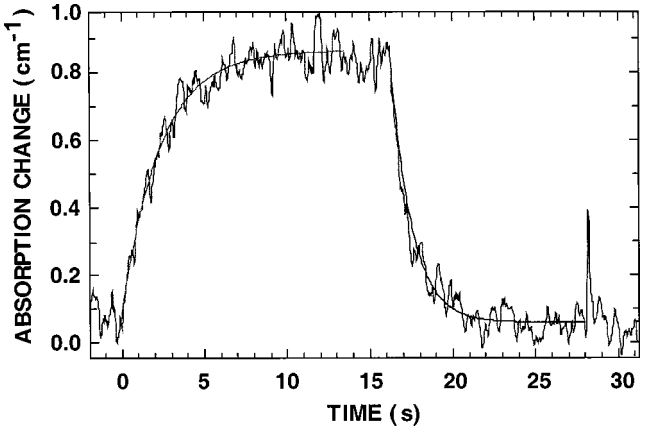

FIG. 5. Light-induced changes in optical absorption at 1.01 μm in $BaTiO_3$:Ce,Rh. At $t = 0$ s an Ar^+-ion laser operating at 488/515 nm was turned on. The absorption rise (rise time = 2.33 s) is due to the generation of new Rh^{4+} centers. When the Ar^+-ion laser beam is turned off at $t = 16.25$ s, the absorption rapidly drops (decay time = 1.26 s) due to photoionization of Rh^{4+} by the 1.01-μm probe.

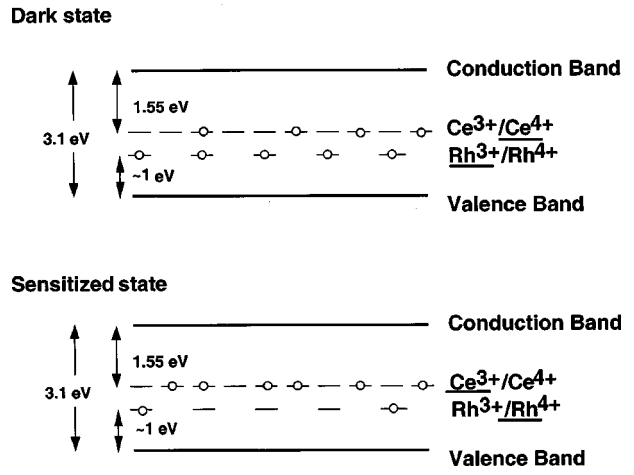

FIG. 6. Schematic band diagram showing the charges during sensitization in $BaTiO_3$:Ce,Rh. Not shown is the Rh^{4+}/Rh^{5+} ionization level located at ~0.7 eV above the valence-band edge; see text for discussion. In the *dark state* the crystal is orange (Ce^{4+}), has a long dark conductivity, and has no sensitivity in the IR. In the *sensitized state*, which persists for many hours, the crystal is blue (Rh^{4+}) and sensitive in the IR. The underlined species identify the predominant valence states.

in the interpretation of the spectroscopic data (see Fig. 6). In a double-doped crystal that has been kept in the dark and in which the Fermi level is located near midgap, Rh is expected to be predominantly in the 3+ valence state, and Ce is likely be present in a mixed 3+/4+ valence state. (Note that the Fermi level can be modified by altering the Ce/Rh ratio and/or by annealing the crystal in an atmosphere with reduced oxygen partial pressure.) This is because the Rh^{3+}/Rh^{4+} ionization level lies close to 1 eV above the valence-band edge and the Ce^{3+}/Ce^{4+} ionization level lies close to midgap, at about 1.5 eV. As long as the Fermi level is pinned to the Ce^{3+}/Ce^{4+} ionization level, the crystal has an orange color typical of pure Ce-doped crystals.[32,33] In addition, the Rh centers are filled with electrons, i.e., in the Rh^{3+} state (in the dark). Thus, the Rh centers have no sensitivity in the IR (which only results from charge-transfer transitions of Rh^{4+} and Rh^{5+}), but will absorb in the blue (around 450 nm) due to ionization of Rh^{3+}. Note that since the Fermi level is pinned near midgap, the Rh^{4+}/Rh^{5+} ionization level located at ~0.7 eV above the valence-band edge is fully populated. This means that there is a fairly low concentration of Rh^{5+} present in our as-grown Ce,Rh-doped crystals. In order to keep the band-energy diagram depicted in Fig. 6 simple, we have chosen not to show the Rh^{4+}/Rh^{5+} ionization level. However, under nonequilibrium conditions as occurs under illumination, Rh^{5+} and other unidentified species may contribute as sources of carriers and traps. We include them, where appropriate, in the discussion that follows.

When the crystal is illuminated with radiation in the blue-green spectral region, two types of transitions can result in the conversion of Rh^{3+} to Rh^{4+}. First, Ce^{4+} can be ionized, with the resulting hole recombining with a Rh^{3+} ion. Second, Rh^{3+} can be ionized, with the resulting electron recombining with Ce^{4+}. Rh^{4+} absorbs over a broad band centered at around 640 nm and extending beyond 900 nm. Thus, blue-green illumination induces the presence of Rh^{4+} centers which are then available to be photoionized by red or near-infrared light. The additional absorption from Rh^{4+} centers results in a very noticeable change in the color of the crystal. In our double-doped crystals, we have observed that effective sensitization can be produced by laser light at 488/515 nm or by ordinary room lighting and that the sensitized state persists for 1–2 days in the dark. We have also observed that illumination of a sensitized crystal in the red or infrared converts the crystal back to its dark state, which is insensitive in the IR.

In order for the grating written at a wavelength in the near-IR to be stable against erasure during readout, the charge distribution generated by the writing beams must reside in the midgap (Ce) level, which is nearly insensitive to infrared radiation. Thus, the grating created via photoionization of an initially homogeneous distribution of charges on the Rh center (in the sensitized state) must be transferred to the Ce centers.

In analogous fashion to the mechanism described by Buse, Adibi, and Psaltis[12] for Fe and Mn in $LiNbO_3$ charges excited from the Rh centers may recombine with Ce centers. The efficient transfer of charge may be enhanced by simultaneous illumination with the sensitizing and writing beams. After the sensitizing beam is turned off, however, the write beams continue to deplete the Rh centers of holes until this level is completely empty (of holes). After this, the charge stored in the Ce centers will be extremely insensitive to erasure by readout light. Alternatively, any remaining charges in the Rh centers will be depleted by thermal ionization, a process which has a decay time of around 10 h in $BaTiO_3$:Rh. We also note that the grating stored in Ce centers is extremely insensitive to dark erasure, with a decay time of ~2000 years demonstrated in $BaTiO_3$:Ce.[10]

A similar sensitizing effect was previously described for a nominally undoped $BaTiO_3$ crystal by Buse, Holtmann, and Krätzig.[8] They found that illumination of $BaTiO_3$ with green light produces new centers sensitive to photoionization by infrared light. In their experiments, however, the identity of the centers involved was not known, and the effect was very short lived.

V. DISCUSSION

A. Ce^{3+} EPR

Theoretical values for the g factors $g_\parallel$ and $g_\perp$ of the spin Hamiltonian given in Eq. (1) can in principle be calculated using the expressions[20]

$$g_\parallel = 2\langle J\|\Lambda\|J\rangle\langle\psi_+|\mathbf{J}_z|\psi_+\rangle, \tag{7}$$

$$g_\perp = \langle J\|\Lambda\|J\rangle\langle\psi_+|\mathbf{J}_+|\psi_-\rangle, \tag{8}$$

where $\langle J\|\Lambda\|J\rangle$ is the Landé factor reduced matrix element and ψ_+ and ψ_- are the two components, for example, of the Kramers's doublet of an ion with an odd number of electrons such as Ce^{3+}.

In C_{3v} symmetry, the ground level $F_{5/2}$ ($J=\frac{5}{2}$) of Ce^{3+} splits into three Kramers's doublets. Two of the doublets transform as ${}^2\Gamma_4$ and the other as ${}^1\Gamma_5 \oplus {}^1\Gamma_6$. The ground state has ${}^2\Gamma_4$ symmetry and in first order, the kets $|\psi_\pm\rangle$ are

linear combinations of the $|J,J_z\rangle$ basis functions $|\frac{5}{2},+\frac{1}{2}\rangle$ and $|\frac{5}{2},-\frac{5}{2}\rangle$. The first-order kets lead to expressions for $g_\parallel$ and $g_\perp$ that are simple functions of the admixture coefficients $\cos\vartheta$ and $\sin\vartheta$. We found, however, that there was no single value of ϑ that gives $g_\parallel$ and $g_\perp$ in exact agreement with experiment. It should be pointed out that recent EPR data for Ce^{3+} in strontium barium niobate $Sr_xBa_{1-x}Nb_2O_6$ (SBN), a host that may be considered similar to $BaTiO_3$, was reported by Giles *et al.*[34] These workers observed a single broad resonance at $g=0.90$.

The discrepancy between the calculated and experimental g factors for Ce^{3+} in various hosts has been considered by Reynolds *et al.*[35] These authors suggest that in order to improve the agreement it is necessary to include admixtures of the excited level $^2F_{7/2}$ in the ground level $^2F_{5/2}$ (recall that the $^2F_{7/2}$ level lies within $\sim$2200 cm^{-1} of the ground state). A mechanism is provided by the static crystal-field potential which, since it contains terms in A_6^6 (crystal-field parameter), leads to mixing of levels differing in J_z by ± 6. Thus, for example, admixture from $|J=\frac{7}{2},J_z=\pm\frac{7}{2}\rangle$ may be realized. This is in line with what was reported for Nd^{3+} in $BaTiO_3$,[19] where it was found that calculation of the g factors requires a ground-level wave function that included an admixture of the excited $^2F_{7/2}$ level.

A feature of the work of Reynolds *et al.*[35] that is also relevant here is that they reported the EPR of Ce^{3+} located at sites of cubic symmetry. The observed g factors were in the range of 0.79 to 0.93, depending on the host. This suggests that Ce^{3+} in $BaTiO_3$ is also located at a site with cubic or nearly cubic symmetry. Based on ionic size considerations we suggest that Ce^{3+} is located on the Ba^{2+} sublattice with a full complement of coordinated oxygen ions.

B. Photo-EPR

Photo-EPR spectra provide insight into the charge transport processes taking place during illumination. Here we describe our observations and then interpret the results in terms of the various reactions that may be involved. Our intent is to attach a chemical label to the species involved in charge generation and/or trapping.

The results shown in curve *a* of Fig. 7 were obtained with the crystal held in the dark for a few hours, after it had previously been exposed to room lights. The EPR spectrum taken along the [001] direction of the sample in this state displayed signals from Rh^{4+} ($\sim$4600 G) and Ce^{3+} ($\sim$5400 G). During illumination with 754-nm light (curve *b*), both signals essentially disappeared. When the light was turned off (curve *c*), the Ce^{3+} signal returned to approximately its original amplitude, whereas the Rh^{4+} signal was virtually absent. This indicates that illumination with 754-nm light effectively resulted in a transfer of charge such that Rh^{4+} was depleted, presumably via conversion to the Rh^{3+} valence state. Subsequently (Fig. 7, curve *d*), the same sample was illuminated by 488/515-nm light from an Ar^+-ion laser. During illumination, the Ce^{3+} signal was absent and a moderate Rh^{4+} signal was observed. When the light was turned off (curve *e*), the Ce^{3+} signal returned to its original amplitude and the Rh^{4+} signal was significantly stronger than before. Thus charge was transferred in such a way as to create additional Rh^{4+} centers. We note that additional unidentified

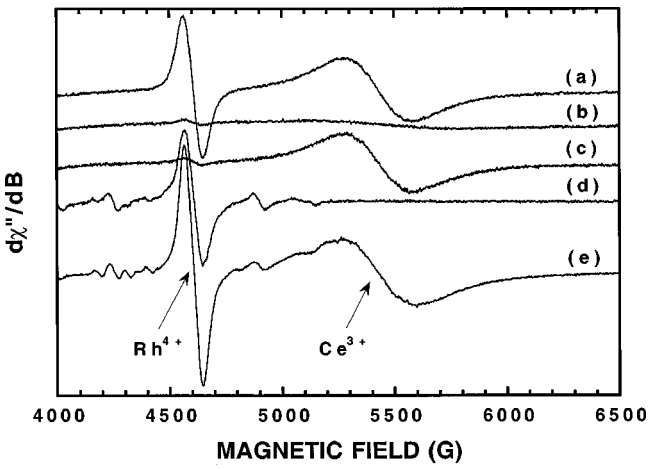

FIG. 7. EPR spectra of a $BaTiO_3$:Ce,Rh crystal (a) before illumination with 754-nm light: (b) under 754-nm illumination; (c) after 754-nm light is turned off; (d) subsequent illumination with 488/515-nm light; and (e) after 488/515-nm light is turned off. All spectra were recorded at $T\sim 15$ K and with $\mathbf{B}\|[001]$ direction. The sample was held at $\sim$15 K throughout the course of these measurements.

centers were also observed as a result of illumination and complicate the interpretation of the results, but are not believed to alter the essential features discussed below.

We suggest that the following set of photoionization, recombination, and trapping processes are operative during illumination:

$$Rh^{4+}+\hbar\omega\rightarrow Rh^{3+}+h_{VB}^{+}, \tag{9}$$

$$Rh^{5+}+\hbar\omega\rightarrow Rh^{4+}+h_{VB}^{+}, \tag{10}$$

$$Ce^{3+}+\hbar\omega\rightarrow Ce^{4+}+e_{CB}^{-}, \tag{11}$$

$$Ce^{3+}+h_{VB}^{+}\rightarrow Ce^{4+}, \tag{12}$$

$$Rh^{4+}+e_{CB}^{-}\rightarrow Rh^{3+}, \tag{13}$$

$$Rh^{4+}+h_{VB}^{+}\rightarrow Rh^{5+}, \tag{14}$$

$$Rh^{5+}+e_{CB}^{-}\rightarrow Rh^{4+}, \tag{15}$$

$$D^{+}+e_{CB}^{-}\rightarrow D, \tag{16}$$

$$A^{-}+h_{VB}^{+}\rightarrow A. \tag{17}$$

In these equations $\hbar\omega$ is the photon energy, e_{CB}^{-} and h_{VB}^{+} represent an electron in the conduction band and a hole in the valence band, respectively, and $\{D,D^+\}$ and $\{A,A^-\}$ correspond to the two states of unidentified shallow donor (D center) and shallow acceptor (A center) defects, respectively.

The holes and electrons released under illumination at 754 nm can be trapped at shallow centers (A and D centers) as well as at the deep centers (Rh and Ce centers). When the 754-nm light is turned off, the Ce^{3+} EPR spectrum returns to its original intensity, whereas the Rh^{4+} spectrum is not observed (see Fig. 7, curve *c*). This suggests that charge carriers e_{CB}^{-} are thermally released and subsequently trapped at Ce^{4+} centers according to the reverse of the reactions given

in Eqs. (11) and (16). During subsequent illumination at low temperatures with 488/515-nm light, a strong Rh^{4+} EPR signal is observed (see Fig. 7, curve *d*); however, the Ce^{3+} is not detected. A set of reactions consistent with this observation includes Eqs. (10), (11), (16), and (17) given above along with

$$Rh^{3+} + \hbar\omega \rightarrow Rh^{4+} + e^{-}_{CB}, \tag{18}$$

$$Ce^{4+} + \hbar\omega \rightarrow Ce^{3+} + h^{+}_{VB}, \tag{19}$$

$$Rh^{4+} + \hbar\omega \rightarrow Rh^{5+} + e^{-}_{CB}, \tag{20}$$

$$Rh^{3+} + h^{+}_{VB} \rightarrow Rh^{4+}. \tag{21}$$

When the 488/515-nm light is turned off, the Ce^{3+} EPR signal returns to roughly its original intensity, while the Rh^{4+} grows to a larger intensity than when under illumination (see Fig. 7, curve *e*). This suggests that carriers are thermally released from the shallow levels and subsequently trapped at the deep levels. This is described by the reaction

$$Ce^{4+} + e^{-}_{CB} \rightarrow Ce^{3+}, \tag{22}$$

and those given in Eqs. (15) and (21) and the reverse of the reactions shown in Eqs. (16) and (17).

Although the present observations are insufficient to determine quantitatively the relative importance of the various processes described above, the overall set of equations presented here should provide a framework for understanding the mechanism of charge redistribution resulting from both thermal and optical excitations. A complete understanding of these processes is key to optimizing the material for use in holographic or other applications.

C. Modification of the Fermi level in $BaTiO_3$:Ce,Rh

These results suggest that $BaTiO_3$:Ce,Rh might be used to record gratings that are relatively insensitive to erasure at the recording wavelength, a possibility supported by grating erasure measurements carried out on a $BaTiO_3$:Ce,Rh crystal.[11] As was also pointed out by these authors, the performance of the material can potentially be improved by optimizing the amplitude of the grating stored in the midgap level. The space-charge field associated with gratings recorded in the Ce centers depends upon the ratio of filled and empty Ce traps, i.e., the Ce^{3+}/Ce^{4+} ratio. Changing the Ce^{3+}/Ce^{4+} ratio corresponds to adjusting the Fermi level in the crystal, as long as the Fermi level lies close to the Ce^{3+}/Ce^{4+} ionization level near midgap. This ratio can be modified via postgrowth processing, by heating the crystal in an atmosphere with a controlled oxygen partial pressure.[36] Reducing the oxygen partial pressure results in a higher Fermi level, corresponding to an increase in the number of traps filled with electrons.

We have carried out preliminary experiments that demonstrate that the Fermi level can in fact be raised by annealing

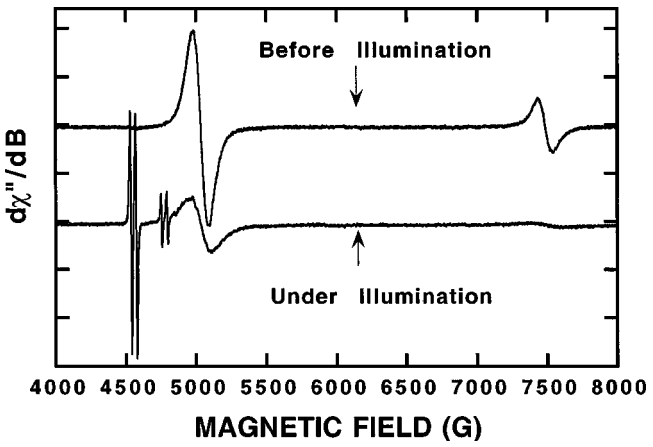

FIG. 8. EPR spectra recorded at $T = 10$ K of $BaTiO_3$:Ce,Rh with $\mathbf{B} \| [111]$ direction. The crystal was annealed in a reducing atmosphere and was only briefly exposed to ambient light prior to the measurements.

$BaTiO_3$:Ce,Rh in a reducing atmosphere. A sample was heated at 700 °C for 20 h in an atmosphere of 50% CO + 50% CO_2, corresponding to an oxygen partial pressure of $\sim 10^{-21}$ bar (the total pressure was ~1 bar). Following this heat treatment, the sample had the characteristic color of $BaTiO_3$:Ce,[33] and we did not observe any color change as a result of exposure to room light. This result demonstrates that the reduction treatment effectively filled the traps involved in charge-transfer processes responsible for the sensitization process in the as-grown crystal. This result suggests that Ce^{4+} centers are in fact involved in the sensitization process and that the Ce^{3+}/Ce^{4+} ratio can be modified by reduction.

We also used EPR methods to study several samples that were annealed at 700 °C in CO-CO_2 atmospheres. The oxygen partial pressure of these experiments ranged from approximately 10^{-6} bar to 10^{-21} bar at the annealing temperature. Shown in Fig. 8 are superimposed EPR spectra obtained on a sample treated at $P_{O_2} = 10^{-21}$ bar before any illumination and then again during illumination with blue-green light from an Ar^{+}-ion laser. Prior to illumination, the only features apparent are those centered at ~5000 and ~7500 G. These features are both due to Ce^{3+}. During illumination the intensity of these features decreases substantially and new spectral lines (doublets) appear centered near 4550 and 4770 G. These features are both due to Rh^{4+}. When the illumination is turned off the Ce^{3+} features return to approximately the same magnitude as before illumination, while the Rh^{4+} features grow slightly stronger than they appear during illumination. On the other hand, a sample annealed at 10^{-6} bar showed strong Rh^{4+} and Ce^{3+} features prior to illumination. These results are consistent with a shift of the Fermi level to a higher position upon reduction, as was also indicated by the change in visible light sensitivity noted above. Interestingly, illumination with an Ar^{+}-ion beam is still able to induce significant charge transfer even in the highly reduced crystal.

These experiments demonstrate that the Fermi level can in fact be adjusted by appropriate annealing treatments, and therefore we believe that optimization of the space-charge field in the deep level, as discussed above, is possible. Fur-

ther experiments are required to find the optimum conditions for the reduction process. In addition, adjustment of the absolute and relative concentrations of the dopants, Ce and Rh, could improve the efficiency of the recording process.

Finally, some comments concerning the shallow *D*- and *A*-centers are in order. In a recent paper Scharfschwerdt *et al.*[37] describe the Fermi-level engineering of $BaTiO_3$:Rh by codoping with sodium. Incorporation of sodium leads to an acceptor level $(Na_{Ba}^{+})'$ that is located ~50 meV above the valence-band edge (here we use the Kröger-Vink notation to indicate the defect charge state relative to the perfect lattice). This acceptor level, which is negatively charged with respect to the lattice, is compensated by the positively charged oxygen vacancy center $V_O^{\bullet\bullet}$ located just below the conduction-band edge. By processing this codoped crystal in a strongly oxidizing atmosphere, these authors[37] report that the Fermi level can be lowered to the Rh^{4+}/Rh^{5+} level. Two points need to made here: (1) drastic conditions are required in order to achieve a reasonable concentration of Rh^{5+}; and (2) unintentional impurities such as alkali-metal ions, as well as other metal contaminants, which lead to shallow acceptor levels, are reasonable candidates for the *A* centers alluded to above. These require compensation, possibly by oxygen vacancies $V_O^{\bullet\bullet}$, which are reasonable candidates for the shallow donor levels (*D* centers).

VI. CONCLUSIONS

Spectroscopic characterization provides some insight at the atomic level into charge-transfer mechanisms in $BaTiO_3$ double-doped with cerium and rhodium. This material displays potential for nonvolatile holographic storage applications using a two-step recording technique. In this technique, two photons of different wavelengths are used for writing; whereas nondestructive readout of the stored information is accomplished using only one of these wavelengths. Optical and EPR measurements have provided information concerning the charge states, electronic structure, and location of the ionization levels associated with the Ce and Rh centers relative to the band edges of the $BaTiO_3$ host. A detailed analysis of the EPR spectra of Ce^{3+} in $BaTiO_3$ has been carried out. Modification of the charge states of the dopant ions as a result of illumination has been studied using photo-EPR and light-modified optical-absorption techniques. A qualitative model of the sensitization process has also been presented, along with a discussion of possible approaches for optimizing $BaTiO_3$:Ce,Rh crystals for nonvolatile holographic recording applications.

Note added in proof: A recent report by Adibi, Buse, and Psaltis [Appl. Phys. Lett. **74**, 3767 (1999)] discussed the effects of oxidation-reduction processing on the storage properties of double-doped $LiNbO_3$ and presented results consistent with the ideas suggested here for optimizing $BaTiO_3$.

ACKNOWLEDGMENTS

The authors thank Marvin Klein for helpful and insightful discussions. We also thank G. D. Bacher and C. C. Nelson for assistance in obtaining optical data and R. G. Wilson for assistance in obtaining SIMS data. This research was supported jointly by Hughes Internal Research and Development funds and by the Defense Advanced Research Projects Agency (DARPA) Photorefractive Information Storage Materials (PRISM) Consortium through Contract No. MDA972-94-2-0008.

*Present address: Crystal Associates, 31 Farinella Drive, East Hanover, NJ 07936.

[1] F. S. Chen, J. T. LaMacchia, and D. B. Fraser, Appl. Phys. Lett. **13**, 223 (1968).
[2] J. F. Heanue, M. C. Bashaw, and L. Hesselink, Science **265**, 749 (1994).
[3] D. Kirillov and J. Feinberg, Opt. Lett. **16**, 1520 (1991).
[4] T. W. McNamara, S. G. Conahan, I. Mnuskhina, M. H. Garrett, H. P. Jenssen, and C. Warde, in *SPIE Critical Review Proceedings*, edited by P. Yeh (SPIE Optical Engineering Press, Bellingham, WA, 1994), Vol. CR-48.
[5] D. Zhang, Y. Zhang, C. Li, Y. Chen, and Y. Zhu, Appl. Opt. **34**, 5241 (1995).
[6] F. Micheron and G. Bismuth, Appl. Phys. Lett. **20**, 79 (1972).
[7] R. S. Cudney, J. Fousek, M. Zgonik, P. Günter, M. Garrett, and D. Rytz, Appl. Phys. Lett. **63**, 3399 (1993).
[8] K. Buse, L. Holtmann, and E. Krätzig, Opt. Commun. **85**, 183 (1991).
[9] Y. S. Bai and R. Kachru, Phys. Rev. Lett. **78**, 2944 (1997).
[10] G. D. Bacher, M. P. Chiao, G. J. Dunning, M. B. Klein, C. C. Nelson, and B. A. Wechsler, Opt. Lett. **21**, 18 (1996).
[11] B. A. Wechsler, M. B. Klein, R. N. Schwartz, and G. D. Bacher, U.S. Patent No. 5,847,851 (Dec. 8, 1998).
[12] K. Buse, A. Adibi, and D. Psaltis, Nature (London) **393**, 665 (1998).
[13] D. L. Staebler and W. Phillips, Appl. Phys. Lett. **24**, 268 (1974).
[14] V. Belruss, J. Kalnajs, A. Linz, and R. C. Folweiler, Mater. Res. Bull. **6**, 899 (1971).
[15] D. Rytz, B. A. Wechsler, C. C. Nelson, and K. W. Kirby, J. Cryst. Growth **99**, 864 (1990).
[16] S. H. Wemple, M. DiDomenico, and I. Camlibel, J. Phys. Chem. Solids **29**, 1797 (1968).
[17] E. Possenriede, P. Jacobs, and O. F. Schirmer, J. Phys.: Condens. Matter **4**, 4719 (1992).
[18] B. A. Wechsler, M. B. Klein, C. C. Nelson, and R. N. Schwartz, Opt. Lett. **19**, 536 (1994).
[19] E. Possenriede, O. F. Schirmer, and G. Godefroy, Phys. Status Solidi B **161**, K55 (1990).
[20] A. Abragam and B. Bleaney, *Electron Paramagnetic Resonance of Transition Ions* (Oxford University Press, London, 1970).
[21] L. Carlsson, Acta Crystallogr. **20**, 459 (1966).
[22] H. Kröse, R. Scharfschwerdt, O. F. Schirmer, and H. Hesse, Appl. Phys. B: Lasers Opt. **61**, 1 (1995).
[23] H. Kröse, E. Possenriede, R. Scharfschwerdt, T. Varnhorst, O. F. Schirmer, H. Hesse, and C. Kuper, Opt. Mater. **4**, 153 (1995).
[24] J. S. Griffith, *The Theory of Transition-Metal Ions* (Cambridge University Press, London, 1961).
[25] C. K. Jørgensen, Acta Chem. Scand. **10**, 500 (1956).
[26] C. K. Jørgensen, Acta Chem. Scand. **11**, 151 (1957).
[27] A. Raizman, J. T. Suss, and S. Szapiro, Phys. Lett. **32A**, 30 (1970).
[28] D. Bravo, M. J. Martín, J. Gavaldá, F. Díaz, C. Zaldo, and F. J. López, Phys. Rev. B **50**, 16 224 (1994).
[29] M. G. Townsend, J. Chem. Phys. **41**, 3149 (1964).
[30] C. K. Jørgensen, Mol. Phys. **5**, 271 (1962).

[31] C. K. Jørgensen and J. S. Brinen, Mol. Phys. **6**, 629 (1963).
[32] K. Binnemans and C. Görller-Walrand, Chem. Phys. Lett. **235**, 163 (1995).
[33] C. Yang, Y. Zhang, P. Yeh, Y. Zhu, and X. Wu, Opt. Commun. **113**, 6 (1995).
[34] N. C. Giles, J. L. Wolford, G. J. Edwards, and R. Uhrin, J. Appl. Phys. **77**, 976 (1995).
[35] R. W. Reynolds, Y. Chen, L. A. Boatner, and M. M. Abraham, Phys. Rev. Lett. **29**, 18 (1972).
[36] B. A. Wechsler and M. B. Klein, J. Opt. Soc. Am. B **5**, 1711 (1988).
[37] R. Scharfschwerdt, O. F. Schirmer, H. Hesse, and D. Rytz, Appl. Phys. B: Lasers Opt. **68**, 807 (1999).